

Research paper

On the dynamics of a spinning top under the influence of rotation: Resonant relative equilibrium states

H. Sheheitli^{a,*}, J.R. Touma^b^aDepartment of Industrial & Mechanical Engineering, Lebanese American University, Byblos, Lebanon^bDepartment of Physics, American University of Beirut, Beirut, Lebanon

ARTICLE INFO

Article history:

Received 12 June 2017

Revised 18 November 2017

Accepted 28 November 2017

Available online 5 December 2017

Keywords:

Spinning top

Nonlinear resonance

Resonance capture

Attitude control

Rotation forcing

Bifurcation

ABSTRACT

We investigate the dynamics of a spinning top driven by a turntable that rotates with a given angular speed Ω . The pivot point of the top is at a fixed distance from the center of the turntable. We show that such a setup leads to resonance where the spinning top is locked in a state of relative equilibrium: precessing with an angular speed equal to that of the turntable while maintaining a constant nutation angle. Bifurcation diagrams are presented to depict how the stability of these relative equilibria, along with the corresponding value of the nutation angle, depends on the two parameters: the initial spin angular momentum and Ω . We discuss the classical spinning top, that is, the $\Omega = 0$ case, and address the relation of the “sleeping top” state to the aforementioned relative equilibria. We also relate the dynamics to that of a spherical pendulum on a rotary arm and show that the latter can be viewed as a special case of the system at hand. Finally, we illustrate how the relative equilibria can be exploited for the attitude control of the top through resonance capture while slowly varying the turntable angular speed, Ω .

© 2017 Elsevier B.V. All rights reserved.

1. Introduction

In 1857, James Clerk Maxwell said [12]: To those who study the progress of exact science, the common spinning top is a symbol of the labors and perplexities of men who had threaded successfully the mazes of planetary motion. The mathematician of the last (XVIII.) century, searching through nature for problems worthy of his analysis, found in the toy of youth ample occupation for the highest mathematical powers”. Indeed, volumes have been written on spinning top dynamics [6–9] and its technological applications. One particular area of application of spinning top dynamics is the study of spacecraft attitude dynamics and control [11]. In this latter context, the rigid body under study is often locked into orbit due to the influence of a central gravitational field. Another field with ubiquitous mention of spinning top dynamics is the study of celestial mechanics. In fact, we are all living on a blue spinning top locked in orbit around the sun. It is well known that celestial spinning bodies are often locked in spin-orbit resonance in what are known as Cassini states [2]. In those states, the spinning body maintains a constant nutation angle relative to the normal to its plane of orbit. Inspired by this, we here consider a toy model problem of a spinning top under the influence of rotational forcing, that is, a spinning top that is pinned at a fixed distance from the center of a turntable that rotates with a constant prescribed angular speed Ω .

* Corresponding author.

E-mail addresses: hiba.sheheitli@lau.edu.lb, hs497@cornell.edu (H. Sheheitli).

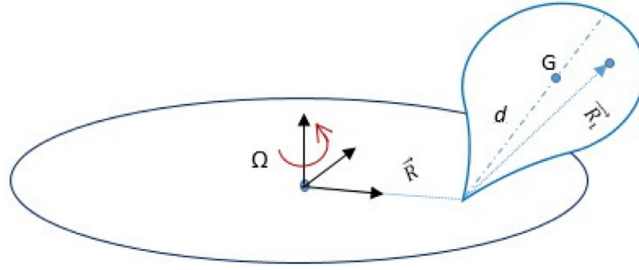


Fig. 1. Schematic of the top on turntable.

We believe this toy model can serve to shed light on interesting dynamical phenomena that may arise from the interplay of rotational and gyroscopic effects in rigid body dynamics.

Closely related to the toy model at hand are problems of pendula under the influence of rotation, often used to illustrate different control techniques [3,4]. While the pendula in these latter works were planar pendula, Ghigliazza and Holmes [5] have analyzed the full nonlinear problem of a spherical pendulum on a rotary arm. The spherical pendulum was found to possess relative equilibrium states in which it precesses at the same speed as that of the rotating arm [5]. Two types of such relative equilibria were reported: a first type in which the pendulum points outwards away from the center of the rotary arm and a second type in which the pendulum points inwards towards the center (see Fig. 4 in [5]). One state of the first type exists and corresponds to the pendulum making an angle $0 < \theta_{e_0} < \pi/2$ from the downward vertical. Whereas, three states of the second type exist: the folded states with $0 < \theta_{e_1} \leq \theta_{e_2} < \pi/2$ and the inverted state with $\pi/2 < \theta_{e_3} < \pi$. The stability of these relative equilibria is studied in [5] and it's shown that θ_{e_0} is always stable while θ_{e_2} and θ_{e_3} are always unstable. θ_{e_1} can be either stable or unstable, depending on system parameters.

We will here show that the spinning top under rotation also possesses these two types of relative equilibria, and while for the pendulum stable states always correspond to a downward pointing position, the spinning top can sustain relative equilibrium states with an upright tilted position, which we refer to as “skewed sleeping top” states. In Section 2, we derive the equations of motions for the system. In Section 3, we look for relative equilibrium states in which the spinning top is locked at constant nutation and precessing at angular speed Ω , that is, it appears to have no precessional motion when viewed in the turntable frame of reference. Section 3.1 presents bifurcation diagrams illustrating how the stability of these relative equilibria and their corresponding value of nutation angle depend on the two parameters: spin angular momentum (p_ψ) and Ω . While an exhaustive study of the full parameter space is left for future work, results for sample ranges for these parameters are presented to shed light on the main features of the dynamics. In Section 4.1, we draw the connection between the results and the special case of the classical “sleeping top”. Then in Section 4.3, we show that the dynamics of the spherical pendulum on a rotary arm are present here for special parameter values. Finally, in Section 5, we illustrate how the attitude of the top can be driven to prescribed values by slowly varying the turntable speed, Ω .

2. The equations of motion

Consider a top of mass M , pivoted to a turning table at a distance R from the center of the table. The center of mass (G) of the top is at a distance d from the pivot point, along the long axis of the top, as shown in schematic of Fig. 1.

2.1. The Lagrangian

The position vector of points on the body can be written as: $\vec{r}_i = \vec{R} + \vec{R}_i$ where $\vec{R} = R\hat{i}$ is the position vector of the pivot point which is fixed to the turntable rotating with angular frequency Ω . $\hat{i}, \hat{j}, \hat{k}$ are orthonormal unit vectors in a frame of reference that rotates with the table. Let $\vec{\Omega}$ and $\vec{\omega}$ be the angular velocity vectors of the turntable and top, respectively. Then, $\vec{\Omega} = \Omega\hat{k} \neq 0$ and $\vec{\omega} = \vec{\omega}_b + \vec{\Omega}$, where $\vec{\omega}_b \neq 0$ is the angular velocity vector of the top relative to the body frame of reference (i.e. a frame of reference rotating with the top). $\vec{\omega}_b$ can be written in terms of the Euler angles (ϕ, θ, ψ) and their derivatives as:

$$\vec{\omega}_b = (\omega_1, \omega_2, \omega_3) \text{ with } \begin{cases} \omega_1 = \dot{\phi} \sin \theta \sin \psi + \dot{\theta} \cos \psi \\ \omega_2 = \dot{\phi} \sin \theta \cos \psi - \dot{\theta} \sin \psi \\ \omega_3 = \dot{\phi} \cos \theta + \dot{\psi} \end{cases}$$

where $0 \leq \theta \leq \pi$, $0 \leq \phi \leq 2\pi$ and $0 \leq \psi \leq 2\pi$. The kinetic energy of the turning top is then given by $T = \frac{1}{2} \int (v_i)^2 dm$, where the integral is over the whole volume of the body and the velocity vector for a mass element of the body, v_i , can be written as:

$$\vec{v}_i = \frac{d\vec{r}_i}{dt} = \frac{d\vec{R}}{dt} + \frac{d\vec{R}_i}{dt} = \vec{\Omega} \times \vec{R} + \vec{\omega} \times \vec{R}_i$$

We expand the expression for the kinetic energy:

$$T = \frac{1}{2} \int [(\vec{\Omega} \times \vec{R}) \cdot (\vec{\Omega} \times \vec{R}) + 2(\vec{\Omega} \times \vec{R}) \cdot (\vec{\omega}_b \times \vec{R}_i) + 2(\vec{\Omega} \times \vec{R}) \cdot (\vec{\Omega} \times \vec{R}_i) + (\vec{\omega}_b \times \vec{R}_i) \cdot (\vec{\omega}_b \times \vec{R}_i) + 2(\vec{\omega}_b \times \vec{R}_i) \cdot (\vec{\Omega} \times \vec{R}_i) + (\vec{\Omega} \times \vec{R}_i) \cdot (\vec{\Omega} \times \vec{R}_i)] dm$$

We have:

$$\begin{aligned} \int (\vec{\Omega} \times \vec{R}) \cdot (\vec{\Omega} \times \vec{R}) dm &= MR^2 \Omega^2 \\ \int (\vec{\Omega} \times \vec{R}) \cdot (\vec{\omega}_b \times \vec{R}_i) dm &= (\vec{\Omega} \times \vec{R}) \cdot (\vec{\omega}_b \times M\vec{d}) = M[(\vec{\Omega} \cdot \vec{\omega}_b)(\vec{R} \cdot \vec{d}) - (\vec{\Omega} \cdot \vec{d})(\vec{R} \cdot \vec{\omega}_b)] \\ \int (\vec{\Omega} \times \vec{R}) \cdot (\vec{\Omega} \times \vec{R}_i) dm &= (\vec{\Omega} \times \vec{R}) \cdot (\vec{\Omega} \times M\vec{d}) = \Omega^2 (\vec{R} \cdot M\vec{d}) \\ \int (\vec{\omega}_b \times \vec{R}_i) \cdot (\vec{\omega}_b \times \vec{R}_i) dm &= \vec{\omega}_b \cdot \int \vec{R}_i \times \vec{\omega}_b \times \vec{R}_i dm = \vec{\omega}_b \cdot \vec{\omega}_b \\ \int (\vec{\omega}_b \times \vec{R}_i) \cdot (\vec{\Omega} \times \vec{R}_i) dm &= \vec{\Omega} \cdot \int \vec{R}_i \times \vec{\omega}_b \times \vec{R}_i dm = \vec{\Omega} \cdot \vec{I} \vec{\omega}_b \\ \int (\vec{\Omega} \times \vec{R}_i) \cdot (\vec{\Omega} \times \vec{R}_i) dm &= \Omega^2 \int (\vec{R}_i \times \hat{k}) \cdot (\vec{R}_i \times \hat{k}) dm = \Omega^2 I_{zz} \end{aligned} \tag{1}$$

In the simplification, we made use of the following equalities:

$$\int \vec{R}_i dm = M\vec{d} \quad \& \quad \int \vec{R}_i \times \vec{\omega}_b \times \vec{R}_i dm = \vec{I} \vec{\omega}_b$$

\vec{I} and I_{zz} denote the moment of inertia tensor of the top about its pivot point and its moment of inertia about a vertical axis through its pivot, respectively. We have:

$$\vec{I} = \begin{bmatrix} I_{xx} & I_{xy} & I_{xz} \\ I_{yx} & I_{yy} & I_{yz} \\ I_{zx} & I_{zy} & I_{zz} \end{bmatrix} = A \begin{bmatrix} I_1 & 0 & 0 \\ 0 & I_2 & 0 \\ 0 & 0 & I_3 \end{bmatrix} A^T$$

where I_1, I_2 & I_3 are the principal moments of inertia of the top and A represents the linear transformation from the table frame of reference to the body frame of reference: ($c \equiv \cos, s \equiv \sin$)

$$A = \begin{bmatrix} c\psi c\phi - c\theta s\phi s\psi & c\psi s\phi + c\theta c\phi s\psi & s\psi s\theta \\ -s\psi c\phi - c\theta s\phi c\psi & -s\psi s\phi + c\theta c\phi c\psi & c\psi s\theta \\ s\theta s\phi & -s\theta c\phi & c\theta \end{bmatrix}$$

Such that:

$$I_{zz} = I_1 \sin^2 \theta + I_3 \cos^2 \theta$$

Also:

$$\frac{1}{2} \vec{\omega}_b \cdot \vec{I} \vec{\omega}_b = \frac{1}{2} (I_1 \omega_1^2 + I_2 \omega_2^2 + I_3 \omega_3^2)$$

We transform $\vec{\Omega}$ and \vec{R} into the body frame of reference and with $\vec{d} = (0, 0, 1)$, we evaluate the dot products appearing in Eq. (1) to obtain the following expression for the kinetic energy of the top:

$$\begin{aligned} T &= \frac{1}{2} I_1 (\dot{\phi}^2 \sin^2 \theta + \dot{\theta}^2) + \frac{1}{2} I_3 (\dot{\phi} \cos \theta + \dot{\psi})^2 + \frac{1}{2} MR^2 \Omega^2 + MR\Omega d (\dot{\phi} \sin \theta \sin \phi - \dot{\theta} \cos \theta \cos \phi) \\ &\quad + \left(\frac{1}{2} \Omega^2 + \Omega \dot{\phi} \right) (I_1 \sin^2 \theta + I_3 \cos^2 \theta) + \Omega \dot{\psi} I_3 \cos \theta + MRd \Omega^2 \sin \phi \sin \theta \end{aligned} \tag{2}$$

Here, we have assumed the top to be axisymmetric with $I_1 = I_2$.

The gravitational potential energy of the top is given by $V = Mgd \cos \theta$, then the Lagrangian is:

$$\begin{aligned} L &= \frac{1}{2} I_1 (\dot{\phi}^2 \sin^2 \theta + \dot{\theta}^2) + \frac{1}{2} I_3 (\dot{\phi} \cos \theta + \dot{\psi})^2 + \frac{1}{2} MR^2 \Omega^2 + MR\Omega d (\dot{\phi} \sin \theta \sin \phi - \dot{\theta} \cos \theta \cos \phi) \\ &\quad + \left(\frac{1}{2} \Omega^2 + \Omega \dot{\phi} \right) (I_1 \sin^2 \theta + I_3 \cos^2 \theta) + \Omega \dot{\psi} I_3 \cos \theta + MRd \Omega^2 \sin \phi \sin \theta - Mgd \cos \theta \end{aligned} \tag{3}$$

2.2. Hamilton's equations

The generalized momenta corresponding to $\phi, \theta,$ and $\psi,$ respectively, are:

$$p_\phi = \frac{\partial L}{\partial \dot{\phi}} = (\dot{\phi} + \Omega) (I_1 \sin^2 \theta + I_3 \cos^2 \theta) + I_3 \dot{\psi} \cos \theta + MR\Omega d \sin \theta \sin \phi$$

$$\begin{aligned}
 p_\theta &= \frac{\partial L}{\partial \dot{\theta}} = I_1 \dot{\theta} - MR\Omega d \cos \theta \cos \phi \\
 p_\psi &= \frac{\partial L}{\partial \dot{\psi}} = I_3 (\dot{\psi} + \dot{\phi} \cos \theta)
 \end{aligned}
 \tag{4}$$

The Hamiltonian is then given by:

$$\begin{aligned}
 H = \dot{\phi} p_\phi + \dot{\theta} p_\theta + \dot{\psi} p_\psi - L &= \frac{1}{2} I_1 (\dot{\phi}^2 \sin^2 \theta + \dot{\theta}^2) + \frac{1}{2} I_3 (\dot{\phi} \cos \theta + \dot{\psi})^2 - \frac{1}{2} \Omega^2 (I_1 \sin^2 \theta + I_3 \cos^2 \theta + MR^2) \\
 &\quad - MRd\Omega^2 \sin \phi \sin \theta + Mgd \cos \theta
 \end{aligned}
 \tag{5}$$

From Eq. (4), we obtain expressions for $\dot{\phi}$, $\dot{\theta}$ & $\dot{\psi}$ in terms of p_ϕ , p_θ & p_ψ :

$$\begin{aligned}
 \dot{\phi} &= \frac{(p_\phi - p_\psi \cos \theta)}{I_1 \sin^2 \theta} - \frac{MR\Omega d \sin \phi}{I_1 \sin \theta} - \Omega \\
 \dot{\theta} &= \frac{1}{I_1} [p_\theta + MR\Omega d \cos \theta \cos \phi] \\
 \dot{\psi} &= \left(\frac{1}{I_3} + \frac{\cos^2 \theta}{I_1 \sin^2 \theta} \right) p_\psi - \frac{\cos \theta}{I_1 \sin^2 \theta} p_\phi + \frac{MR\Omega d \cos \theta \sin \phi}{I_1 \sin \theta}
 \end{aligned}$$

Substituting the above expressions into Eq. (5), we obtain the Hamiltonian in terms of the Euler angles and the corresponding conjugate momenta:

$$\begin{aligned}
 H &= \frac{1}{2I_1} p_\theta^2 + \frac{1}{2I_3} p_\psi^2 + \frac{1}{2I_1 \sin^2 \theta} (p_\phi - p_\psi \cos \theta)^2 - \frac{MR\Omega d}{I_1 \sin \theta} \sin \phi (p_\phi - p_\psi \cos \theta) + \frac{MR\Omega d}{I_1} p_\theta \cos \theta \cos \phi \\
 &\quad + \frac{(MR\Omega d)^2}{2I_1} (\sin^2 \phi + \cos^2 \theta \cos^2 \phi) - \Omega p_\phi - \frac{1}{2} MR^2 \Omega^2 + Mgd \cos \theta
 \end{aligned}$$

Then the resulting Hamilton's equations are:

$$\begin{aligned}
 \dot{\phi} &= \frac{1}{I_1 \sin^2 \theta} (p_\phi - \cos \theta p_\psi - MR\Omega d \sin \phi \sin \theta) - \Omega \\
 \dot{p}_\phi &= \frac{MR\Omega d}{I_1 \sin \theta} \cos \phi (p_\phi - \cos \theta p_\psi) + \frac{MR\Omega d}{I_1} \sin \phi \cos \theta p_\theta - \frac{(MR\Omega d)^2}{I_1} \sin \phi \cos \phi \sin^2 \theta \\
 \dot{\theta} &= \frac{1}{I_1} (p_\theta + MR\Omega d \cos \phi \cos \theta) \\
 \dot{p}_\theta &= \frac{1}{I_1 \sin^3 \theta} [\cos \theta (p_\phi^2 + p_\psi^2) + (\sin^2 \theta - 2) p_\psi p_\phi] + \frac{MR\Omega d}{I_1 \sin^2 \theta} \sin \phi (p_\psi - \cos \theta p_\phi) + \frac{MR\Omega d}{I_1} \cos \phi \sin \theta p_\theta \\
 &\quad + \frac{(MR\Omega d)^2}{I_1} \cos^2 \phi \sin \theta \cos \theta + Mgd \sin \theta \\
 \dot{\psi} &= \left(\frac{1}{I_3} + \frac{\cos^2 \theta}{I_1 \sin^2 \theta} \right) p_\psi - \frac{\cos \theta}{I_1 \sin^2 \theta} p_\phi + \frac{MR\Omega d}{I_1} \sin \phi \frac{\cos \theta}{\sin \theta} \\
 \dot{p}_\psi &= 0
 \end{aligned}$$

The last equation implies that $p_\psi = I_3(\dot{\phi} \cos \theta + \dot{\psi}) = \text{constant}$. The spin angle ψ is a cyclic coordinate and we are left with a 2 degree of freedom system. We non-dimensionalize the equations using: $t \rightarrow \tilde{t}/\Omega$ & $p \rightarrow \tilde{p} p_\psi$. We are assuming here that p_ψ is non-zero, otherwise the dynamics would reduce to that of the spherical pendulum, as discussed later in Section 4.3. After the transformation, the system becomes:

$$\begin{aligned}
 \dot{\phi} &= \frac{1}{\sin^2 \theta} [\alpha (p_\phi - \cos \theta) - \beta \sin \phi \sin \theta] - 1 \\
 \dot{p}_\phi &= \beta \left[\frac{\cos \phi}{\sin \theta} (p_\phi - \cos \theta) + \sin \phi \cos \theta p_\theta \right] - \frac{\beta^2}{\alpha} \sin \phi \cos \phi \sin^2 \theta \\
 \dot{\theta} &= \alpha p_\theta + \beta \cos \phi \cos \theta \\
 \dot{p}_\theta &= \frac{\alpha}{\sin^3 \theta} [\cos \theta (p_\phi^2 + 1) + (\sin^2 \theta - 2) p_\phi] + \beta \frac{\sin \phi}{\sin^2 \theta} (1 - \cos \theta p_\phi) + \beta \cos \phi \sin \theta p_\theta \\
 &\quad + \frac{\beta^2}{\alpha} \cos^2 \phi \sin \theta \cos \theta + \frac{\gamma}{\alpha} \sin \theta
 \end{aligned}
 \tag{6}$$

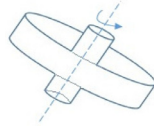


Fig. 2. Schematic of the shape of the spinning top.

Along with the equation for the spin angular velocity:

$$\dot{\psi} = \alpha \left[\left(r_l + \frac{\cos^2 \theta}{\sin^2 \theta} \right) - \frac{\cos \theta}{\sin^2 \theta} p_\phi \right] + \beta \sin \phi \frac{\cos \theta}{\sin \theta} \quad (7)$$

Note that the tilde has been dropped for brevity. The non-dimensional parameters are defined as follows:

$$\alpha = \frac{p_\psi}{I_1 \Omega}, \quad \beta = \frac{MRd}{I_1}, \quad \gamma = \frac{Mgd}{I_1 \Omega^2}, \quad r_l = \frac{I_1}{I_3}$$

3. Relative equilibria

We look for relative equilibrium states in which the top is locked into resonance with the rotation of the turntable, that is, the spinning top precesses at the same angular speed as the turntable ($\dot{\phi} = 0$ or $\phi = \phi^* = \text{constant}$) while maintaining a constant nutation angle $\theta = \theta^*$. Such states correspond to $\dot{\phi} = \dot{p}_\phi = \dot{\theta} = \dot{p}_\theta = 0$. From Eq. (6), we obtain the following conditions to be satisfied:

$$\begin{aligned} \dot{\phi} = 0 &\Rightarrow p_\phi^* = \cos \theta^* + \frac{\beta}{\alpha} \sin \phi^* \sin \theta^* + \frac{1}{\alpha} \sin^2 \theta^* \\ \dot{p}_\phi = 0 &\Rightarrow \cos \phi^* (p_\phi^* - \cos \theta^*) + \sin \phi^* \left(\sin \theta^* \cos \theta^* p_\theta^* - \frac{\beta}{\alpha} \cos \phi^* \sin^3 \theta^* \right) = 0 \\ \dot{\theta} = 0 &\Rightarrow p_\theta^* = -\frac{\beta}{\alpha} \cos \phi^* \cos \theta^* \\ \dot{p}_\theta = 0 &\Rightarrow \cos \theta^* \left((p_\phi^*)^2 + 1 \right) + (\sin^2 \theta^* - 2) p_\phi^* + \frac{\beta}{\alpha} \sin \phi^* \sin \theta^* (1 - \cos \theta^* p_\phi^*) + \frac{\gamma}{\alpha^2} \sin^4 \theta^* \\ &\quad + \frac{\beta}{\alpha} \cos \phi^* \sin^4 \theta^* \left(p_\theta^* + \frac{\beta}{\alpha} \cos \phi^* \cos \theta^* \right) = 0 \end{aligned} \quad (8)$$

The first three conditions above lead to:

$$\cos \phi^* \sin^2 \theta^* = 0 \Rightarrow \phi = \frac{\pi}{2} \text{ or } \frac{3\pi}{2}$$

So we have two families of such relative equilibria which we will denote as equilibria A and B, such that:

$$\phi_A^* = \frac{\pi}{2}, \quad \phi_B^* = \frac{3\pi}{2}$$

This means that in state A, the spin axis of the top points outwards (away from the center of the turntable) in the plane of \vec{k} and \vec{R} , while in state B, it points inwards (towards the center of the turntable) in the same plane. Substituting into the last condition in Eq. (8), we obtain the following equations to be solved for the corresponding values $\theta_{A,B}^*$:

$$f_{A,B}(\theta) = (\gamma - \alpha) \sin \theta + \cos \theta (\sin \theta \pm \beta) = 0 \quad (9)$$

That is, θ_A^* and θ_B^* are solutions to $f_A(\theta) = 0$ and $f_B(\theta) = 0$, respectively, if any exist.

3.1. Bifurcation diagrams

As an example, we choose $R = 2\text{m}$ and the spinning top to have the shape illustrated in Fig. 2, with a 4kg disk of 1m radius and 10cm thickness, and a 0.8kg rod with 20cm radius and 50cm length, leading to the following values for the physical parameters: $I_1 = 1.438 \text{ kg}\cdot\text{m}^2$, $I_3 = 2.016 \text{ kg}\cdot\text{m}^2$, $d = 0.2917 \text{ m}$, $M = 4.8 \text{ kg}$. This results in $\alpha = \frac{0.6954 p_\psi}{\Omega}$, $\beta = 1.9474$ and $\gamma = \frac{9.5519}{\Omega^2}$.

Hence, we explore the dynamics as the two remaining parameters, p_ψ and Ω , vary. Figs. 3 and 4 show bifurcation diagrams, i.e. the value of $\theta_{A,B}^*$ vs. Ω for several values of p_ψ , along with linear stability results. We note here that, for the chosen parameters, θ_B^* takes on a unique value for a given Ω , however, for other parameter values, $f_B(\theta) = 0$ can possibly have two or three solutions; this is further discussed in Section 4.3. It can be seen that θ_A^* is always linearly stable. For large enough p_ψ , θ_B^* is stable in a small window of Ω values (Fig. 3(d)). Within this window of Ω values, linearization

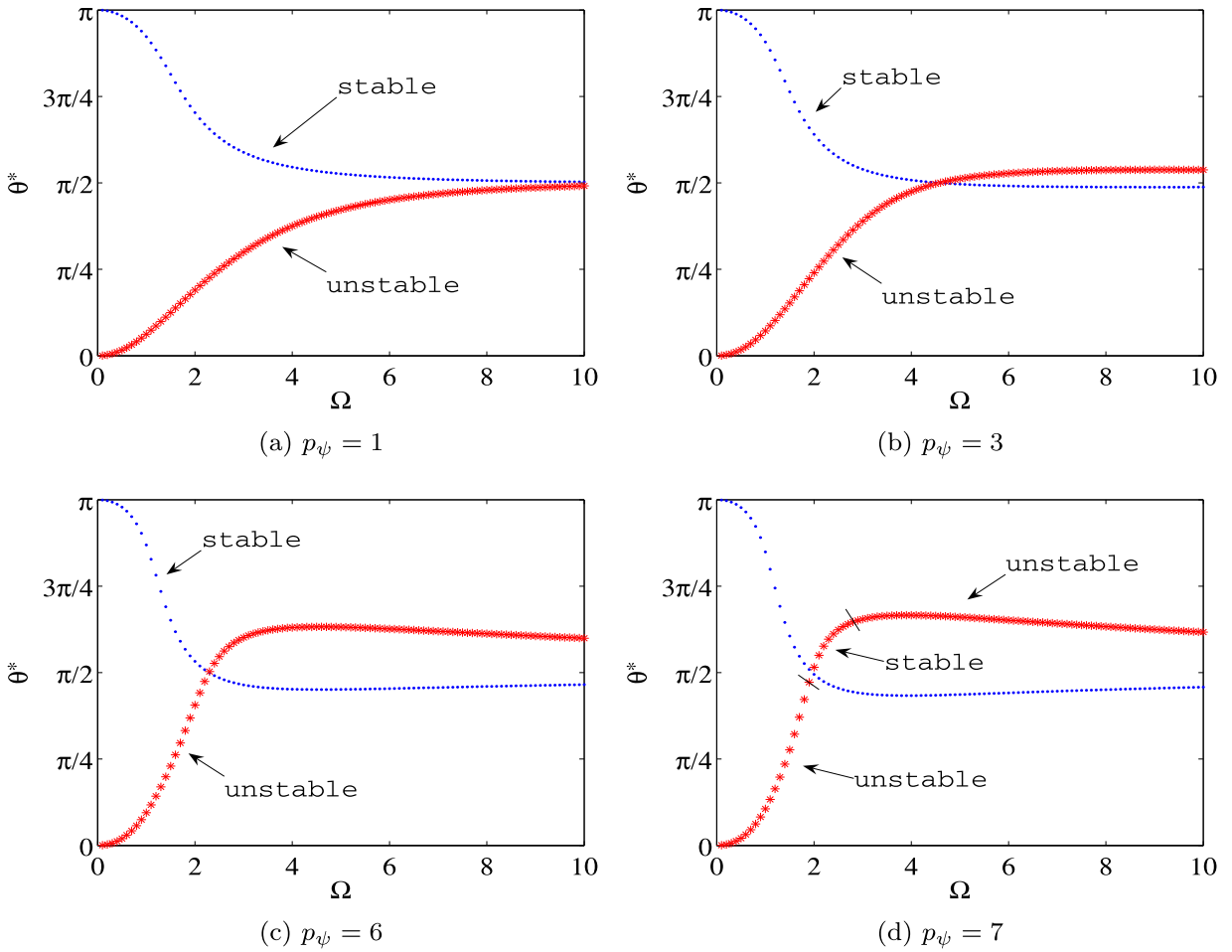


Fig. 3. Bifurcation Diagrams showing the values of θ_A^* (• blue) & θ_B^* (* red) vs. Ω for different values of p_ψ . (For interpretation of the references to colour in this figure legend, the reader is referred to the web version of this article.)

of the system in Eq. (6) at the θ_B^* relative equilibrium state results in a pair of purely imaginary eigenvalues. At the endpoints of the window of stability, the pair of purely imaginary eigenvalues collide and depart from the pure imaginary axis, indicating that the relative equilibrium loses stability through a Hamiltonian Hopf bifurcation [10]. As p_ψ is further increased (Fig. 4(a) and (b)), the window of stability grows larger with the lower endpoint moving towards lower Ω values that correspond to smaller θ_B^* values, eventually reaching zero at the critical value $p_{\psi,0}^c$ defined in the next section.

It is worth noting that, as Figs. 3 and 4 show, $\theta_{A,B}^* \rightarrow \pi/2$ as $\Omega \rightarrow \infty$, however, the $\theta_{A,B}^* = \pi/2$ solution also exists for $\Omega_{\pi/2} = Mgd/p_\psi$; while this is evident in Figs. 3(b)–(d) and 4(a)–(d), it is absent in Fig. 3(a) since the corresponding value of $\Omega_{\pi/2} = 13.7$ lies outside the displayed range of Ω . For validation, Fig. 5 shows the time series for solutions starting with initial conditions that correspond to the predicted relative equilibrium states and hence remain locked at it for all time. Fig. 6 shows the time series for solutions starting in the neighborhood of and far from the relative equilibria. We can see that if we start close enough to one of the stable states, then the top is locked to oscillate about it (Fig. 6(a)–(d)), however, if we start far enough, the top escapes into fully precessional motions (Fig. 6(e) and (f)). These numerical experiments indicate that the system at hand possesses rich and possibly chaotic dynamics, the full study of which is left for future work.

4. Discussion

4.1. The classical spinning top revisited

To interpret the results shown in the bifurcation diagrams, we revisit the classical spinning top problem. For $\Omega = 0$, the equations of motion reduce to:

$$\dot{\phi} = \frac{1}{I_1 \sin^2 \theta} (p_\phi - \cos \theta p_\psi); \dot{p}_\phi = 0$$

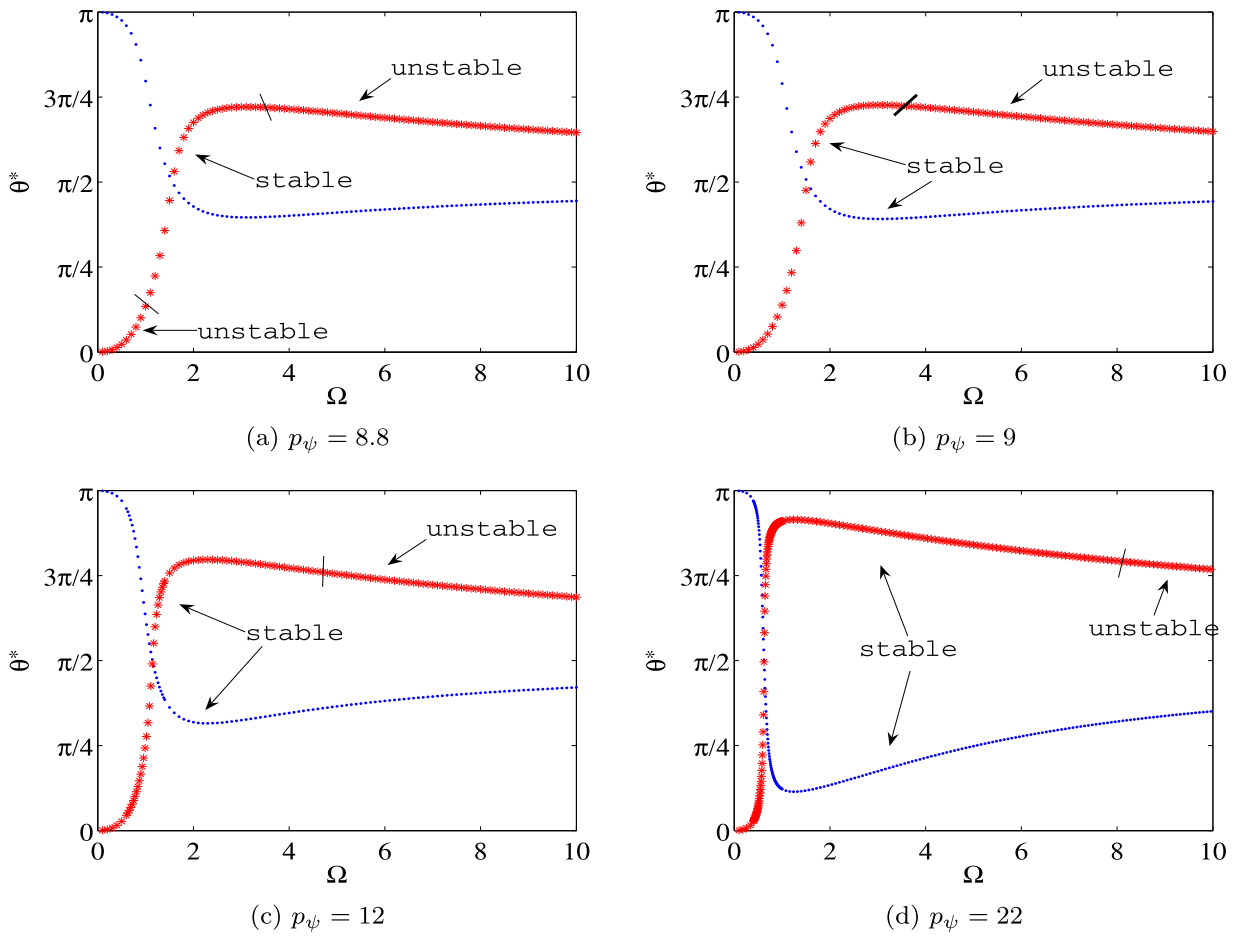


Fig. 4. Same as in Fig. 3.

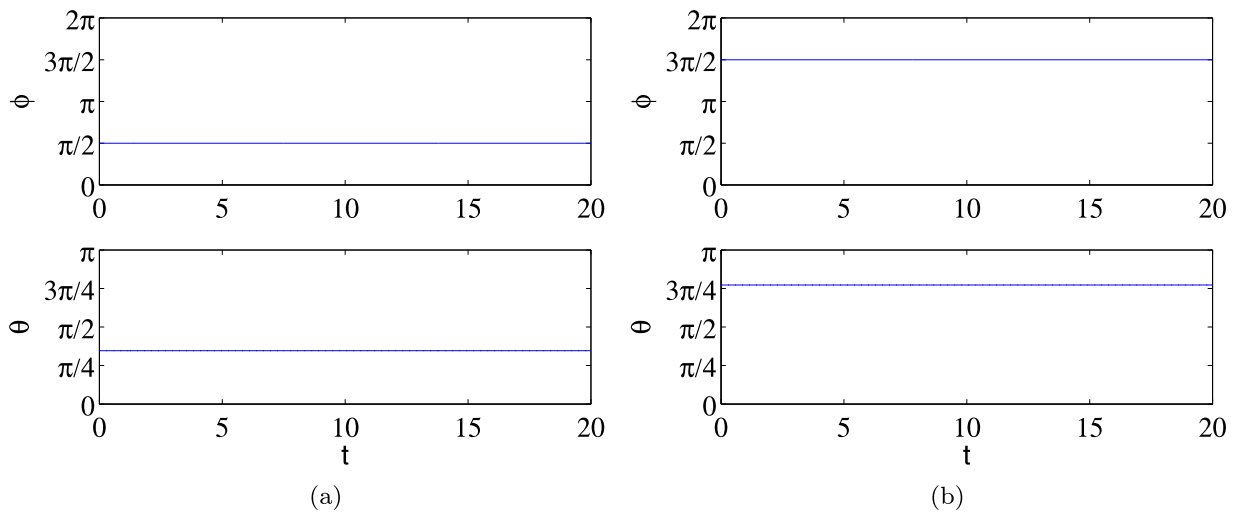


Fig. 5. Time series for integration with $p_\psi = 12$, $\Omega = 4$; the initial condition corresponds to the relative equilibrium state corresponding to (a) $\theta_A^* \approx 1.087$ and (b) $\theta_B^* \approx 2.43$.

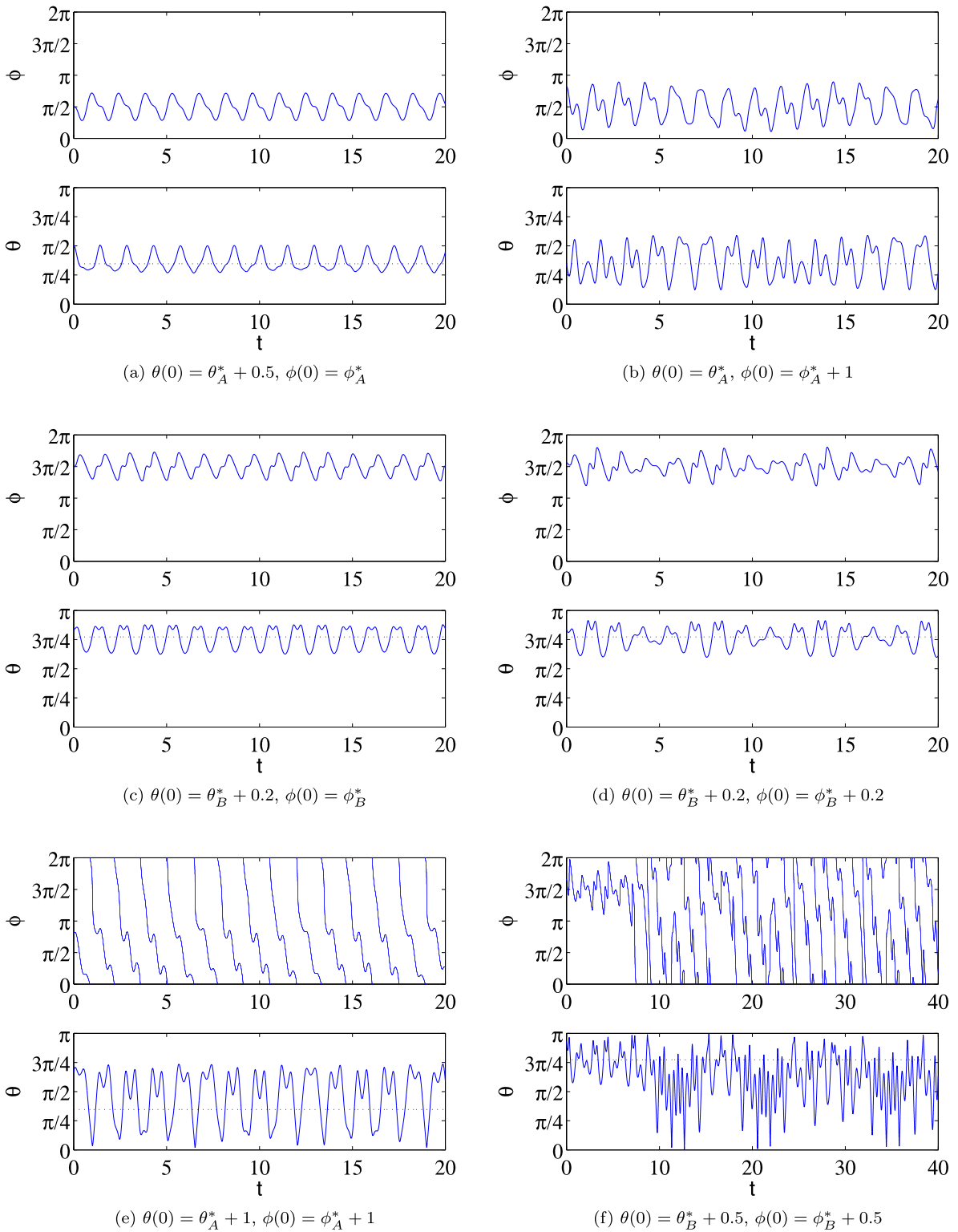


Fig. 6. Time series for integration starting with different initial conditions for $p_\psi = 12, \Omega = 4$.

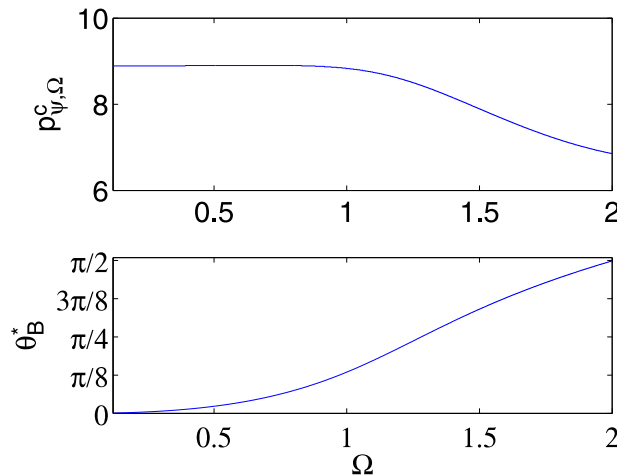


Fig. 7. $p_{\psi, \Omega}^c$ as a function of Ω and the evolution of the corresponding θ_B^* .

$$\dot{\theta} = \frac{1}{I_1} p_\theta$$

$$\dot{p}_\theta = \frac{1}{I_1 \sin^3 \theta} [\cos \theta (p_\phi^2 + p_\psi^2) + (\sin^2 \theta - 2) p_\psi p_\phi] + Mgd \sin \theta$$

$$\dot{p}_\psi = \left(\frac{1}{I_3} + \frac{\cos^2 \theta}{I_1 \sin^2 \theta} \right) p_\psi - \frac{\cos \theta}{I_1 \sin^2 \theta} p_\phi; \quad \dot{p}_\psi = 0$$

with the corresponding Hamiltonian:

$$H = \frac{1}{2I_1 \sin^2 \theta} p_\phi^2 + \frac{1}{2I_1} p_\theta^2 + \frac{1}{2} \left(\frac{1}{I_3} + \frac{\cos^2 \theta}{I_1 \sin^2 \theta} \right) p_\psi^2 - \frac{\cos \theta}{I_1 \sin^2 \theta} p_\psi p_\phi + Mgd \cos \theta$$

Since p_ψ and p_ϕ are conserved, the dynamics reduces to a one degree of freedom system governing θ . This system possesses an equilibrium point at $\theta = 0$, referred to as the “sleeping top” state. It’s known [1] that the “sleeping top” is stable for $p_\psi > p_{\psi, 0}^c$, where

$$p_{\psi, 0}^c = 2\sqrt{MgdI_1}$$

The naming is due to the fact that when dissipation is present, a “sleeping top” spinning at $\theta = 0$ is seen to “awaken” as p_ψ decreases and the top loses its upright position. For the values used in Section 3.1, $p_{\psi, 0}^c \approx 8.88$. This is consistent with what’s seen in the bifurcation diagrams of Fig. 4(a) and (b), in which the lower branch near $\theta = 0$ goes from being unstable at $p_\psi = 8$ to stable at $p_\psi = 9$. In fact, for small enough Ω there exists a critical value $p_{\psi, \Omega}^c$ such that for $p_\psi > p_{\psi, \Omega}^c$, the corresponding θ_B^* relative equilibrium state is stable. This means that the “sleeping top” state persists but with the spin axis pointing inwards towards the center of the orbit with a nutation angle θ_B^* , instead of being vertical as in the $\Omega = 0$ case; we refer to this as the “up-inward sleeping top”. We can see in Fig. 7 that $p_{\psi, \Omega}^c$, obtained from linear stability analysis, decreases as Ω increases.

4.2. Coexistence of two stable “sleeping top” states

It can be inferred from the bifurcation diagrams that when the “up-inward sleeping top” state is stable, it coexists with a “down-outward sleeping top” state that corresponds to the relative equilibrium having a nutation of θ_A^* . Actually, this “down-outward sleeping top” state reduces to the vertically downwards stable equilibrium state at $\theta = \pi$ when $\Omega = 0$. As Ω increases past the intersection point of the two θ^* branches in the bifurcation diagram, the two “sleeping top” states switch sides such that we have an “up-outward sleeping top” state corresponding to θ_A^* and a “down-inward sleeping top” state corresponding to θ_B^* , as illustrated in the schematic in Fig. 8. As Ω is further increased, the θ_B^* relative equilibria eventually loses stability and then the “up-outward sleeping top” is the only remaining stable relative equilibrium.

4.3. Relation to the spherical pendulum on a rotary arm

The ideal spherical pendulum, that is, a particle of mass M on a massless rod of length d , can be viewed as a special case of a spinning top with $I_3 = 0$ and $I_1 = I_2 = Md^2$. Hence, we expect that the results obtained here for a spinning top

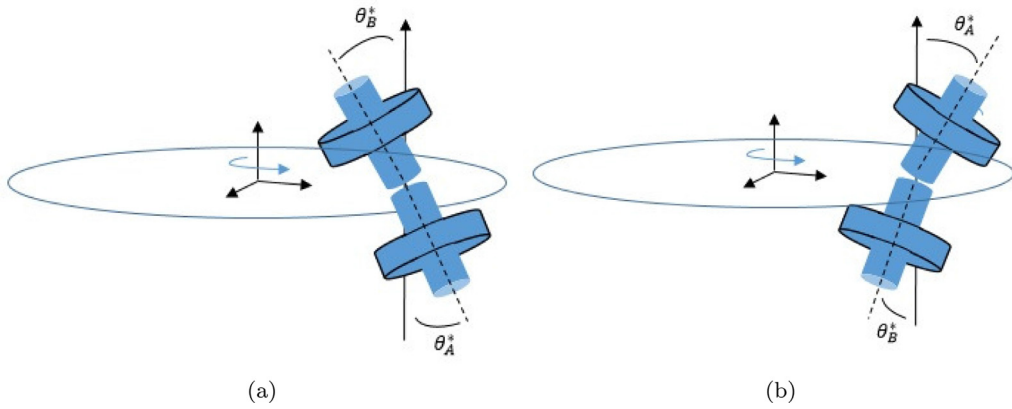


Fig. 8. Stable relative equilibrium states (a) before and (b) after the intersection of the two θ^* curves in the bifurcation diagram.

on a turntable should reduce to that obtained for the spherical pendulum on a rotary arm in [5], if we set $I_3 = 0$ and $I_1 = I_2 = Md^2$. This would lead to $p_\psi = 0$, i.e. $\alpha = 0$ with $\beta = R/d$ and $\gamma = g/(d\Omega^2)$. Indeed, it can be easily verified that the equations of motion obtained here reduce to those in [5] for these parameter values. To avoid confusion, we note that R , d and Ω are denoted as b , l and $\dot{\psi}$, respectively, in [5]. Also, in [5], θ is measured from the downward vertical, whereas here we are following the Euler angles convention in which θ refers to the angle made relative to the upward vertical.

Observe that Eq. (9) can be rewritten as:

$$\sin \theta \pm \beta = (\alpha - \gamma) \tan \theta \tag{10}$$

This reduces exactly to Eq. (23) in [5] for the special case of $\alpha = 0$, $\beta = R/d$ and $\gamma = g/(d\Omega^2)$. This suggests that the bifurcations occurring for the spherical pendulum on a rotary arm might also be present here for the spinning top. While for the parameter values chosen in Figs. 3 and 4, there exists only one θ_B^* value for a given Ω value, for a different range of parameter values, two or three such states might exist, as for the spherical pendulum. To show that, we look for the tangency condition of the two functions appearing on the two sides of Eq. (10):

$$\cos^3 \theta = \alpha - \gamma$$

Substituting this in Eq. (10), we get:

$$\sin^3 \theta = \mp \beta$$

The latter two expressions can be combined into:

$$(\beta)^{2/3} + (\alpha - \gamma)^{2/3} = 1 \tag{11}$$

Recall that $\alpha = \frac{p_\psi}{I_1 \Omega^2}$, $\beta = \frac{MRd}{I_1}$, $\gamma = \frac{Mgd}{I_1 \Omega^2}$.

So we rearrange Eq. (11) to obtain the following quadratic equation in Ω :

$$\pm \left[1 - \left(\frac{MRd}{I_1} \right)^{2/3} \right]^{3/2} \Omega^2 - \frac{p_\psi}{I_1} \Omega + \frac{Mgd}{I_1} = 0 \tag{12}$$

Note that we have two cases, the first corresponds to the tangency occurring for a value of $0 < \theta < \pi/2$ with $\cos \theta > 0$ and the second corresponds to a value of $\pi/2 < \theta < \pi$ with $\cos \theta < 0$. The possible roots of these equations are given by:

$$\Omega_{1,2,3,4} = \pm \frac{1}{2} \left[1 - \left(\frac{MRd}{I_1} \right)^{2/3} \right]^{-3/2} \left(\frac{p_\psi}{I_1} \pm \sqrt{\left(\frac{p_\psi}{I_1} \right)^2 \pm 4 \frac{Mgd}{I_1} \left[1 - \left(\frac{MRd}{I_1} \right)^{2/3} \right]^{3/2}} \right) \tag{13}$$

For a given p_ψ , Eq. (13) gives the value(s) of Ω at which a tangency occurs between the functions on the two sides of Eq. (10), that is, at which a saddle node bifurcation is expected to occur and give rise to two additional θ_B^* relative equilibria. It can be seen that in order to have a real root, we need:

$$\frac{MRd}{I_1} \leq 1$$

For the parameter values used in Figs. 3 and 4, we have $\frac{MRd}{I_1} = 1.947 > 1$, so this condition is not satisfied and we do not see the mentioned bifurcations. Instead, if we choose $R = 1$ which leads to $\frac{MRd}{I_1} = 0.9736 < 1$, then for small enough p_ψ ,

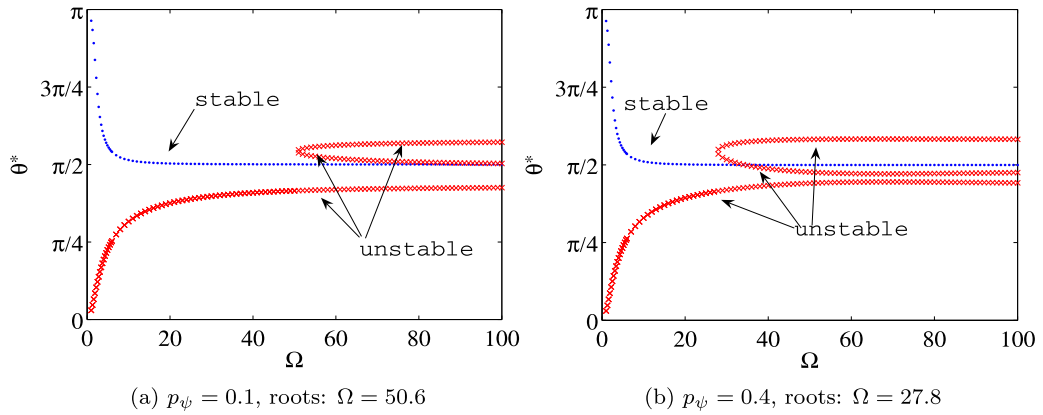


Fig. 9. Bifurcation Diagrams showing the values of θ_A^* (. blue) & θ_B^* (x red) vs. Ω for different values of p_ψ , with $R = 1m$. The corresponding roots of Eq. (12) are given under each figure. (For interpretation of the references to colour in this figure legend, the reader is referred to the web version of this article.)

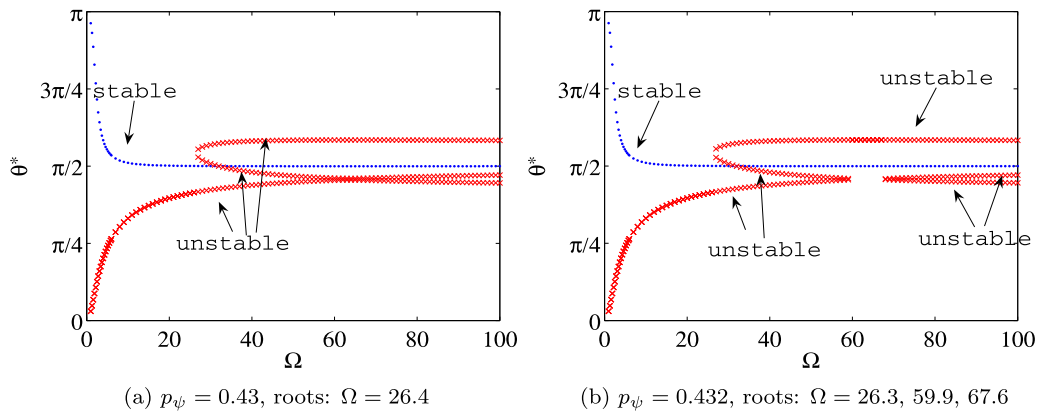


Fig. 10. Same as in Fig. 9.

the resulting bifurcation diagram, shown in Fig. 9, resembles that of the spherical pendulum (see Fig. 5 in [5]). However, in Fig. 10, we can see that as p_ψ is increased, the lower and middle θ_B^* branches approach each other and meet to create a cusp before splitting into two folds. The cusp corresponds to the value of p_ψ at which Eq. (12) has a double root, that is:

$$p_{\psi,d} = 2I_1 \sqrt{\frac{Mgd}{I_1} \left[1 - \left(\frac{MRd}{I_1} \right)^{2/3} \right]^{3/2}}$$

This expression gives $p_{\psi,d} \approx 0.431$ for the parameters used here, which is consistent with what’s seen in Fig. 10.

Note that for the parameter values used in Figs. 9 and 10, the θ_B^* states born out of the saddle node bifurcations are unstable. Fig. 11 illustrates how an even smaller value of R would lead to one of those θ_B^* to be born as stable, before loosing stability through a Hamiltonian Hopf bifurcation as Ω is further increased, just like in the spherical pendulum case. In [5], it’s shown that there is a critical ratio of radius of rotary arm to length of pendulum below which this window of stability exists. Here, the non-dimensional parameter β is analogous to the mentioned ratio, and so we suspect that there is a critical β value below which this window of stability exists, however the large number of parameters present here renders the algebraic analysis required to obtain this condition a rather non-trivial one.

We can see that the spinning top under rotation possesses the main features of the spherical pendulum under the same effect. A major distinction between the two is that the stable relative equilibria of the spherical pendulum are restricted to downward pointing positions, that is, corresponding to $0 < \theta < \pi/2$ from the downward vertical. The presence of the spinning motion, with the right parameter values, gives rise to upwards relative equilibrium states that correspond to $\pi/2 < \theta < \pi$ from the downwards vertical, with the top tilted either towards or away from the center of rotation. We next discuss how this can be exploited to drive a spinning top to a desired attitude.

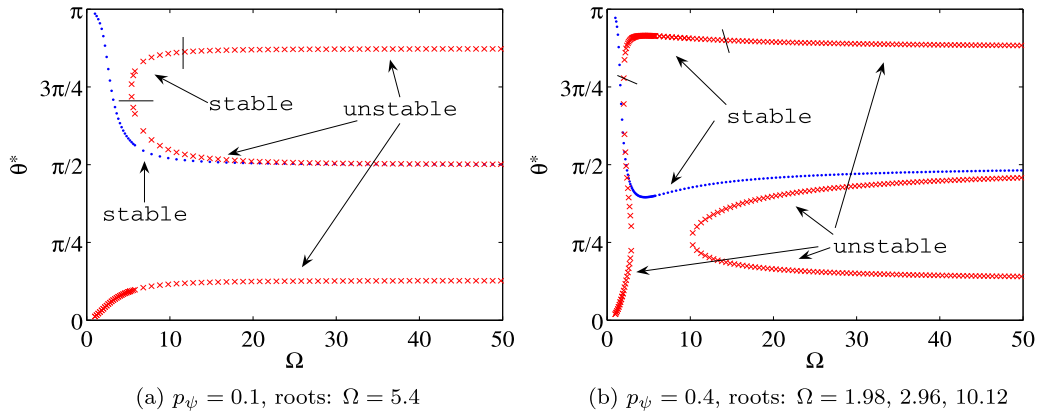


Fig. 11. Bifurcation Diagrams showing the values of θ_A^* (blue) & θ_B^* (x red) vs. Ω for different values of p_ψ , with $R = 0.4m$. The corresponding roots of Eq. (12) are given under each figure. (For interpretation of the references to colour in this figure legend, the reader is referred to the web version of this article.)

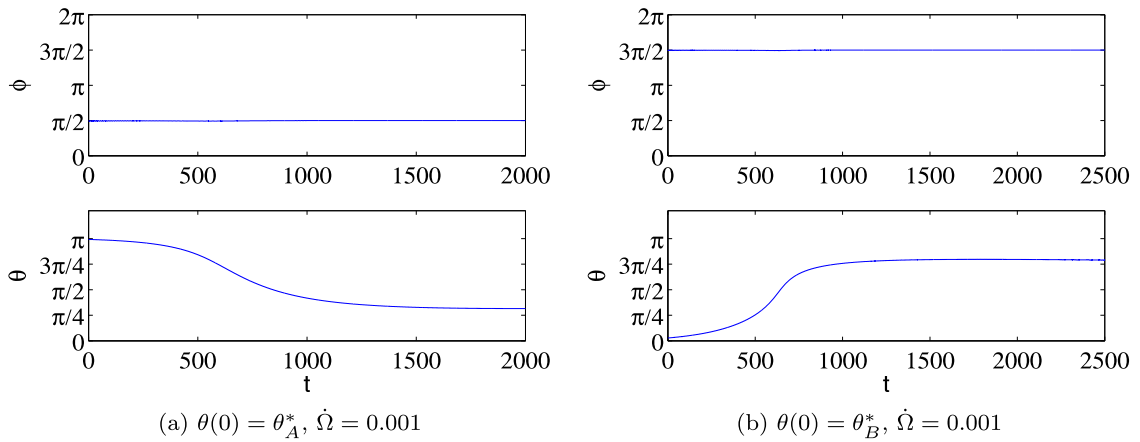


Fig. 12. Numerical experiments demonstrating control of nutation through resonance capture while slowly varying Ω . $p_\psi = 12$.

5. Control through resonance capture

The relative equilibria discussed here correspond to a state of 1:1 resonance between the precession of the top and the rotational forcing. We predict that if the top starts with an initial condition corresponding to one of the stable relative equilibrium states, it will remain captured in resonance if the frequency of rotational forcing is allowed to slowly vary. This will result in the top staying at the initial ϕ^* while θ follows the evolving value of θ^* depicted in the bifurcation diagrams, as illustrated in Fig. 12. In Fig. 13(a) we start with an initial condition corresponding to θ_A^* near the downright position and then linearly increase Ω to 1 which corresponds to $\theta_A^* \approx 2$, we then keep Ω constant at that value and see that the top remains locked at the relative equilibria. Ω is then decreased to take the top back to near downright position. In another numerical experiment shown in Fig. 13(b), after keeping the top at $\theta_A^* \approx 2$ for a period of time, we increase Ω again to take it to $\theta_A^* \approx 1.3$ corresponding to $\Omega = 1.3$. These experiments serve to illustrate how, by the mere slow variation of Ω , the attitude of the top can be prescribed to take desired values while its precession angle remains locked at the chosen value of $\phi^* = \pi/2$ or $3\pi/2$ relative to the turntable.

6. Conclusion

We investigated the dynamics of a spinning top driven by a constant speed rotation and showed the existence of relative equilibrium states in which the spinning top is locked into resonance at a constant nutation angle while precessing at the same speed as that of the rotation of the turntable. We studied the evolution and bifurcations of these states as a function of the parameters p_ψ and Ω . A natural link to the classical spinning top case was made such that these relative equilibria can be thought of as “skewed sleeping top” states. It was also shown that the dynamics of the spherical pendulum on a rotary arm persists for the spinning top for a special range of parameters and that spinning motion allows the relative equilibria to correspond to upward pointing states that are not possible for the simple spherical pendulum. Finally, we

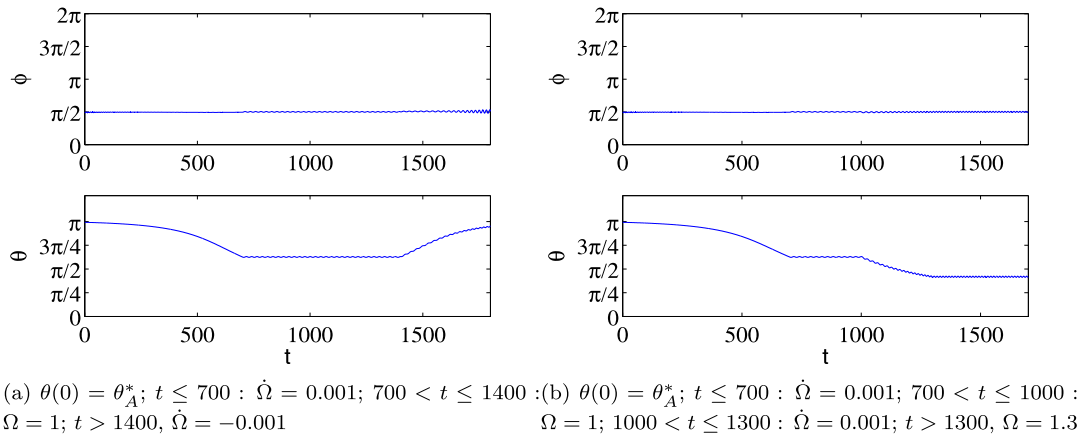


Fig. 13. Same as in Fig. 12.

illustrated how, due to resonance capture, these states offer possibilities for controlling the attitude of the spinning top via slow variation of the rotational speed.

References

- [1] Arnold VI. *Mathematical methods of classical mechanics*. Springer; 1989.
- [2] Beletsky VV. *Essays on the motion of celestial bodies*. Springer Basel AG; 2001.
- [3] Bloch AM, Leonard NE, Marsden JE. Stabilization of the pendulum on a rotor arm by the method of controlled lagrangians. In: *Proceedings of IEEE international conference on robotics and automation*, vol. 1. Detroit, MI; 1999. p. 500–5.
- [4] Furuta K, Yamakita M, Kobayashi S. Swing up control of inverted pendulum. In: *Proceedings of international conference on industrial electronics, control and instrumentation*; 1991. p. 2193–8.
- [5] Ghigliazza RM, Holmes P. On the dynamics of cranes, or spherical pendula with moving supports. *Int J Nonlinear Mech* 2002;37:1211–21.
- [6] Klein F, Sommerfeld A. *The theory of the top. Volume I: introduction to the kinematics and kinetics of the top*. Birkhauser Basel; 2008.
- [7] Klein F, Sommerfeld A. *The theory of the top. Volume II: development of the theory in the case of the heavy symmetric top*. Birkhauser Basel; 2010.
- [8] Klein F, Sommerfeld A. *The theory of the top. Volume III: perturbations. Astronomical and geophysical applications*. Birkhauser Basel; 2012.
- [9] Klein F, Sommerfeld A. *The theory of the top. Volume IV: technical applications of the theory of the top*. Birkhauser Basel; 2014.
- [10] Lahiri A, Roy MS. The Hamiltonian Hopf bifurcation: an elementary perturbative approach. *Int J Nonlinear Mech* 2001;36:787–802.
- [11] Rimrott FPJ. *Introductory attitude dynamics*. New York: Springer-Verlag; 1989.
- [12] Maxwell JC. On a dynamical top, for exhibiting the phenomena of the motion of a system of invariable form about a fixed point, with some suggestions as to the Earth's motion. In: *Transactions of the royal society of Edinburgh*, XXI, part IV; 1857. p. 55970.